J Appl Electrochem (2009) 39:2257–2264
DOI 10.1007/s10800-009-9857-7

ORIGINAL PAPER

Electrochemical performance of Ni-based anodes for solid oxide fuel cells

S. Presto · A. Barbucci · M. P. Carpanese · M. Viviani · R. Marazza

Received: 7 October 2008 / Accepted: 24 February 2009 / Published online: 24 March 2009

Abstract The catalytic activity of Ni-based anodic materials was investigated in complete solid oxide fuel cells (SOFCs) by electrochemical analysis. Button cells, consisting of supporting yttria-stabilized zirconia (YSZ) electrolyte layer, $(La_{1-x}Sr_x)_y$ MnO_3 (LSM) cathode and (cermet) $Ni_{0.5}Co_{0.5}$–YSZ anode were employed. Powders for anodes were obtained by wet impregnation. This procedure allowed easy production of composite electrodes with homogeneous distribution of phases and controlled microstructure. Two electrodes impedance spectroscopy was carried out at different temperatures and partial pressures of reacting gases in order to evaluate contribution of each component to overall cell losses. Current–voltage characteristic curves were also collected. Feeding with CH_4 was tested and compared to H_2. No deterioration of cell performance due to carbon formation at anode was observed over a test period of 100 h.

S. Presto · R. Marazza
Dipartimento di Chimica e Chimica Industriale, Università di Genova, Via Dodecaneso 31, 16146 Genoa, Italy

A. Barbucci · M. P. Carpanese
Dipartimento di Ingegneria Chimica e Processo, Università di Genova, P.le J.F. Kennedy, Pad. D, 16129 Genoa, Italy

S. Presto (✉) · M. Viviani
Istituto per l'Energetica e le Interfasi, CNR, Via De Marini, 6, 16149, Genoa, Italy
e-mail: s.presto@ge.ieni.cnr.it

S. Presto · A. Barbucci · M. P. Carpanese · M. Viviani · R. Marazza
Consorzio Interuniversitario Nazionale per la Scienza e Tecnologia dei Materiali, Via Giusti, 9, 50121 Florence, Italy

Keywords Solid oxide fuel cell · Methane · Ni-based anode · Impedance spectroscopy

1 Introduction

A solid oxide fuel cell (SOFC) is the most efficient electrochemical device for power generation, converting the chemical energy available in fuels like hydrogen, hydrocarbons or synthetic gases into electricity. Not all technological problems have been solved yet and one of the main issues is to lower the operation temperature to 600–700 °C maintaining a reasonably high power density. This task implies the development of electrolytic materials with high ionic conductivity and electrodes with high electrocatalytic activity for hydrogen oxidation and oxygen reduction. In general, important limitations may arise from electrodes behavior. Dealing with hydrogen fuel, voltage losses are mainly due to oxygen reduction and therefore concentrated at the cathode. On the contrary if hydrocarbon fuels are directly injected into the cell, anodic reaction kinetics is likely to become crucial as both fuel reforming and electrocatalytic hydrogen oxidation must be activated. In this case, anode catalytic activity must be enhanced and maintained in spite of possible carbon formation, frequently leading to premature deactivation of the electrode and consequently of the cell [1, 2]. For example when methane is fueled and internal reforming

$$CH_4 + H_2O \rightarrow 3H_2 + CO \quad (1)$$

$$CH_4 + CO_2 \rightarrow 2H_2 + 2CO \quad (2)$$

or direct electrochemical oxidation

$$CH_4 + 2O_2 \rightarrow 2H_2O + CO_2 \quad (3)$$

happens the carbon formation can occur by methane pyrolysis

$$CH_4 \rightarrow C + 2H_2 \quad (4)$$

or carbon monoxide disproportionation

$$2CO \rightarrow C + CO_2 \quad (5)$$

Generally the situation is difficult to predict because the rate of carbon formation or the complete suppression of reactions (4) and (5) strongly depend upon both the thermodynamic and kinetic aspects, particularly by catalytic efficiency of anodic materials, temperature, CO/CO_2 and H_2/H_2O ratio resulting from fuel composition and reactions in the cell. The testing conditions also affect the carbon formation, especially if the electrochemical measurements of SOFC are performed in OCV conditions or with polarization.

Recently, to face the problem of carbon deposition, anodic materials different from Ni-cermet, such as copper [3], doped ceria [4, 5], and alternative other conducting oxides with fluorite, rutile, tungsten bronze pyrochlore, perovskite and spinel structure [6–8] have been studied. Unfortunately, the performance of such anodes tends to be poor compared to that of Ni based anodes because Cu is a very poor electrocatalyst, and the electronic conductivity is lower in oxides than metals. Anyway alternative materials still need optimization before being suitable for replacement of the traditional Ni-based materials. Therefore, Ni-based anodes still appear as attractive candidates for SOFCs if the problem of carbon formation can be overcome. Partial substitution of Ni with Cu, Co and Fe [9–12] has been considered, but, in spite of the great deal of work in this area, the understanding of carbon formation process is still far to be completely clarified. Nevertheless, results on $Ni_{1-x}Co_x$–YSZ cermet anode [12] showed that the cobalt content does not affect the cell performance for hydrogen oxidation and increases the fuel cell performance for feeding with methane and strongly reduces carbon deposition within the anodic layer. The same authors reported the highest activity for the anodic oxidation of methane for the composition $Ni_{0.5}Co_{0.5}$–YSZ. Further confirmations of Co effect on reduction of carbon formation derive also from study on catalytic activity of yttria-stabilized zirconia (YSZ) supported Ni–Co alloys in the steam reforming of ethanol [13]. In that case the methane is an intermediate product of the steam reforming reaction, and the carbon deposition on Ni_xCo_x–YSZ catalyst is less than the case in which YSZ supported Ni catalyst is used. Another crucial aspect is that the electrochemical performance of Ni-YSZ and $Ni_{1-x}M_x$–YSZ (with M = Cu, Co and Fe and $0 < x < 1$) fuel cell anodes are mostly dependent on the microstructure, which is directly related to the properties of starting powder. In particular, homogenous distribution and connectivity of the three phases (metal, oxide and voids) in the final layer have to be ensured, mainly through optimized preparation routes of starting powders. The most common way to get anodic powders is by mechanical mixing of YSZ and NiO precursors. Recently a number of studies about the preparation of enhanced $Ni_{1-x}M_x$–YSZ cermets have been published proposing alternative procedure like: combustion synthesis [14], sol–gel precipitation [15], gel casting technique [16], mechanofusion method [17] and wet impregnation [18–20].

The aim of this work is to prepare Ni-based cermet anodic powders by wet impregnation and to investigate their activity in $Ni_{0.5}Co_{0.5}$–YSZ/YSZ/LSM complete cells, under hydrogen and methane atmosphere.

2 Experimental

2.1 Powders preparation and characterization

Powders with homogeneous distribution of $Ni_{0.5}Co_{0.5}O$ and YSZ were prepared by the wet impregnation technique using commercial 8 mol% yttria-stabilized ZrO_2 powder (TZ-8YS, Tosoh) and the following metal nitrate precursors: $Ni(NO_3)_2 \cdot 6H_2O$ (99%, Carlo Erba Analytical) and $Co(NO_3)_2 \cdot 6H_2O$ (99%, Carlo Erba Analytical). Nitrates were dissolved in distilled water and the proper amount of YSZ was added to provide a final loading of 50 wt% with respect to the metal. Powders were dried for 4 days at 120 °C and subsequently calcined at 400, 600 and 800 °C in air atmosphere. X-ray diffraction measurements (Philips X'Pert, $\lambda_{k\alpha}Cu = 1.5418$ Å) were performed to control the powder composition and the crystallinity. Moreover the microstructure of the powder was observed by scanning electron microscopy (Jeol SM-840).

2.2 Cell preparation and characterization

The cell was of the electrolyte supporting type. Electrolyte was obtained by uniaxial pressing of 2.5 g of Y-stabilized ZrO_2 powder (TZ-8YS Tosoh powder) and sintering in air at 1500 °C for 5 h. The final result was a full dense ceramic disk 2 cm in diameter and about 2 mm thick.

$(La_{1-x}Sr_x)_yMnO_3$ ($x = 0.25$ and $y = 0.95$ Praxair) powder was used to realise the cathode. Both anode and cathode powders were mixed with α-Terpineol (Aldrich) and subsequently painted on the two sides of the electrolyte disk by slurry coating. The anode was sintered in air at 1350 °C for 10 h and subsequently the cathode was applied and sintered in air at 1100 °C for 1 h. After sintering each electrode was 40 ± 3 μm thick and 10 mm in diameter. The thickness was evaluated by SEM observation over the whole section.

Two platinum wires were attached to each electrode with a platinum mesh 10 mm in diameter, used as current collector. The cell was placed in a shielded alumina rig [21], inserted in a tubular furnace and then kept at 700 °C for 24 h. Before performing the measurements the anode was reduced at this temperature in hydrogen atmosphere to obtain a Ni–Co based YSZ cermet. The cells measurements in the two electrode configuration were carried out between 600 and 900 °C. The gas supply on the anode side was hydrogen or methane and on the cathode side was oxygen, eventually diluted with N_2. The anodic gases were humidified by bubbling through water at room temperature, resulting in a nominal water content of 3 wt%. The nominal water vapour partial pressure was estimated by assuming that equilibrium is attained in these condition. The electrochemical investigations consisted of impedance spectroscopy (EIS) and potential dynamic measurements. The electrochemical analyses were performed using a Autolab pgstat 30 (Metrohm) analyzer over the frequency range 0.1 Hz–1 MHz with a 10 mV A.C. signal amplitude in open circuit voltage (OCV) condition.

3 Results and discussion

The morphological aspect of (Ni,Co)O–YSZ powders calcined at 400 °C (a), 600 °C (b) and 800 °C (c) was observed by SEM (Fig. 1) and their structure was analyzed by X-ray diffraction measurements (Fig. 2). The SEM observations confirmed a particle size of the powders with a narrow distribution ranging between 100 and 200 nm with aggregates that maintain a good open porosity. The X-ray patterns display at all temperatures the peaks of YSZ and $Ni_{1-x}Co_xO$. At lower temperatures the phase Co_3O_4 is also present but decomposes after treatment at 800 °C, in accordance with the phase diagram of the system Ni–Co–O [22]. Moreover, increasing calcination temperature there is a growth of both crystallites and agglomerates. In order to have a good homogeneous distribution of Ni and Co and a good crystallinity, the powder calcined at 800 °C was chosen to fabricate anodes. Higher temperatures were not considered for powder synthesis to avoid further increase of particle size. Figure 3a shows a cross section of the anodic side of the cell before reduction. Generally good adhesion of the anode to the electrolyte support and open porosity of the electrode is displayed. However, the anode at this stage seems not to have an elevated porosity. Figure 3b shows a detail of a part of anode that was detached from the cell after that the whole preparation was completed. In this figure is clearly highlighted how the thermal treatments modify the morphology of the anode from the starting powders. In fact the size of the ionic conductor is different with respect to the solid solution of

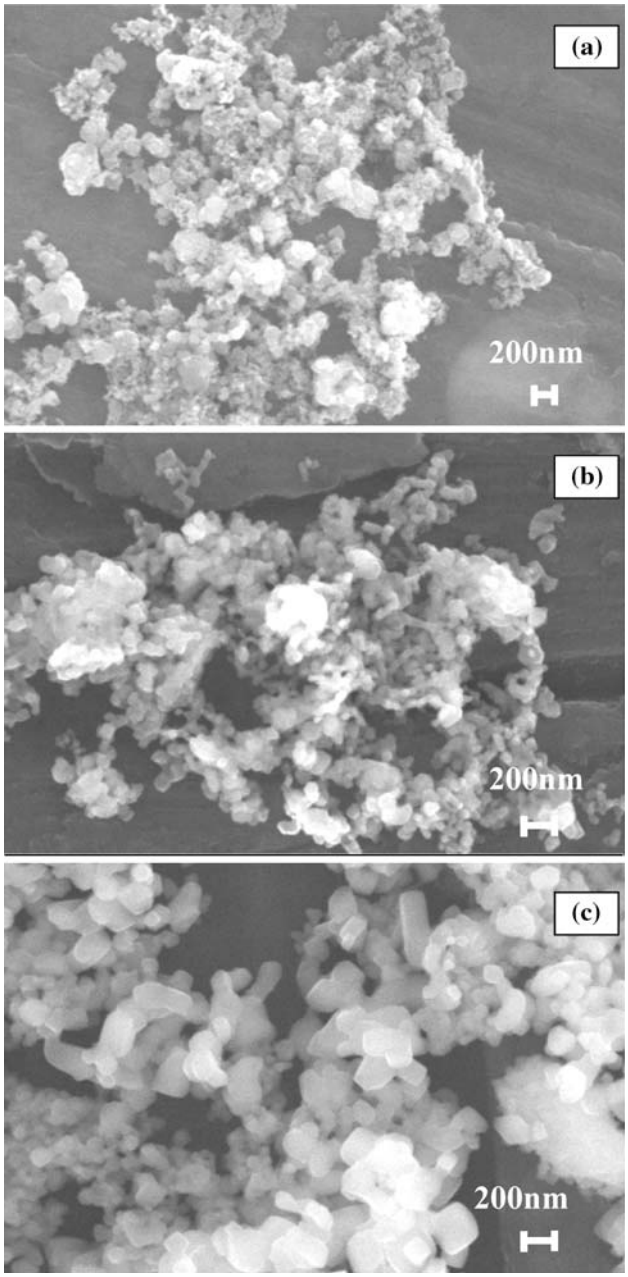

Fig. 1 SEM images of (Ni,Co)O–YSZ powders calcined at 400 °C (**a**), 600 °C (**b**) and 800 °C (**c**)

mixed oxide although the two species are well distributed; small YSZ particles surround agglomerates of the electrocatalyst. To characterize the anode microstructure after electrochemical measurements and evaluate possible morphological change due to the measurements, the cell was cooled down in hydrogen to avoid re-oxidation. Figure 4a shows the aspect of the anode/electrolyte interface cross section as measured by SEM. Moreover in Fig. 4b–d, X-ray maps obtained by EDS on the same sample are also shown: the distribution of three fundamental elements

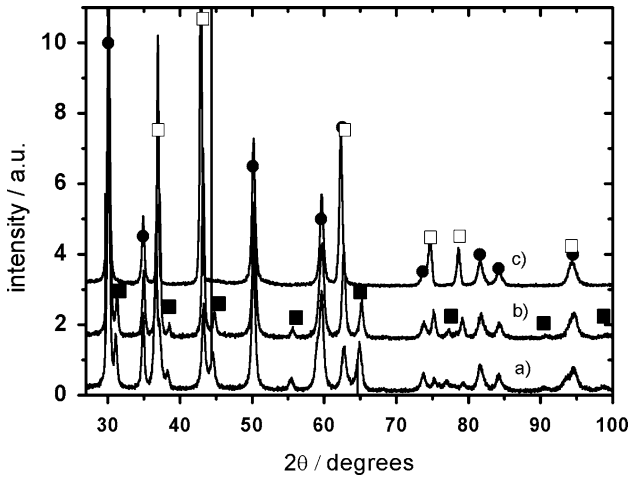

Fig. 2 X-ray diffraction patterns of (Ni,Co)O–YSZ powders calcined at 400 °C (**a**), 600 °C (**b**) and 800 °C (**c**). YSZ (●) and $Ni_{0.5}Co_{0.5}O$ (□) peaks are indicated. In patterns (a) and (b) Co_3O_4 (■) peaks are also present

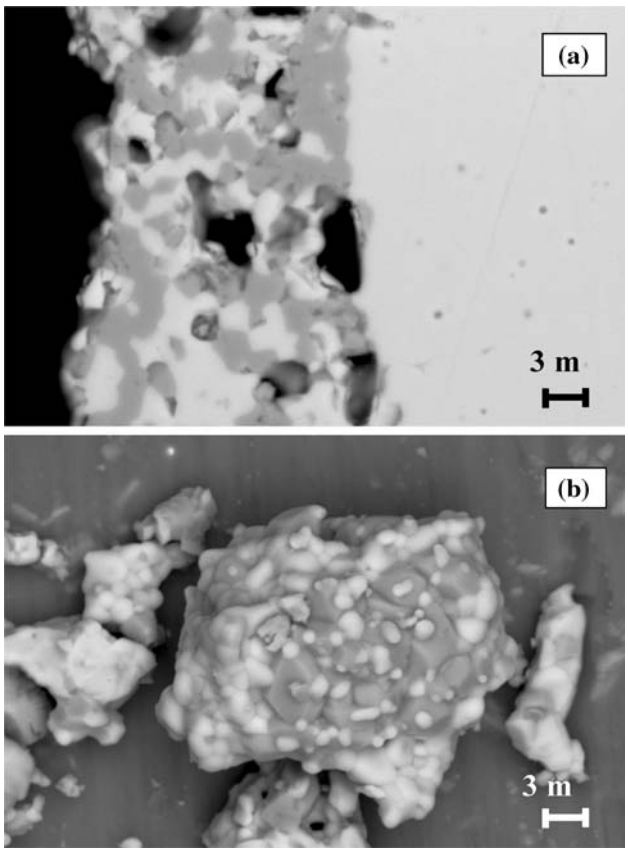

Fig. 3 SEM micrographs. (**a**) Cross section of the anode/electrolyte interface before reduction; (**b**) powder of the anode detached from the cell after that the preparation was completed

(Zr, Co, Ni) is homogeneous along the thickness of the electrode indicating that the ionic and electronic conductor phases are homogeneously mixed in the cermet.

Impedance measurements performed at open circuit voltage on complete cell at 700 °C at different partial pressures are reported in Fig. 5. In particular Fig. 5a shows data collected with constant cathode gas composition (100% O_2) and variable H_2 partial pressure at the anode, while Fig. 5b shows results obtained with constant anode gas composition (100% H_2) and variable O_2 partial pressure at the cathode side. These diagrams suggest that at 700 °C the partial pressure of H_2 does not affect the cell performances, confirming that at this temperature the hydrogen oxidation kinetic of the anodic processes is faster than the cathodic oxygen reduction. Even at very low H_2 partial pressure (0.05 atm) the kinetic of the overall process is not affected by the anodic side of the cell. On the other hand, Nyquist diagrams highlight a large dependence from the partial pressure of O_2 (Fig. 5b), confirming that the global kinetic of the cell is strongly dependent on what happens at the cathode side: the cathodic reaction determines the global response of the system. On the contrary, at higher temperature (800 °C, Fig. 6a, b) the situation changes with the anodic gas composition also affecting the electrochemical response of the system. This fact is ascribed to the enhancement of the electrocatalytic activity of LSM toward oxygen reduction in this temperature range (700–800 °C). At 800 °C the decrease of the hydrogen content in the anodic side results in a slower anodic kinetics that now affects the cell behaviour; the rate of the anodic and cathodic processes are balanced and any modification in only one side of the cell influences its performance.

From these diagrams (Figs. 5, 6) the so called polarization resistance (R_p) was extracted considering the difference between the intercept of the data at low and high frequencies (diameter of the semicircle) and in Fig. 7a the dependence of $\ln(1/R_p)$, on $\ln(p(H)_2)$ is reported for both 700 and 800 °C. The diagram shows that at 700 °C no effect on R_p with hydrogen partial pressure is obtained while at 800 °C $\ln(1/R_p)$, has a clear dependence on $\ln(p(H_2))$. In Fig. 7b the dependence of $\ln(1/R_p)$ on $\ln(p(O_2))$ at 700 °C gives a linear relationship with a slope of 0.35.

Kim et al. [23] in a cathodic half cell configuration studied the dependence of the reaction rate with the oxygen partial pressure considering a model mechanism originally proposed by van Heuveln and Bouwmeester [24]. Kim et al. recognized that in this mechanism when the charge transfer is the rate determining step the overall reaction rate is proportional to the oxygen partial pressure to the 3/8. Which means a slope of the line presented in Fig. 7b equal to 0.37. Furthermore, in a recent experimental and theoretical study [25, 26] it was underlined that with LSM based cathodes at 700 °C the oxygen reduction process is governed by charge transfer.

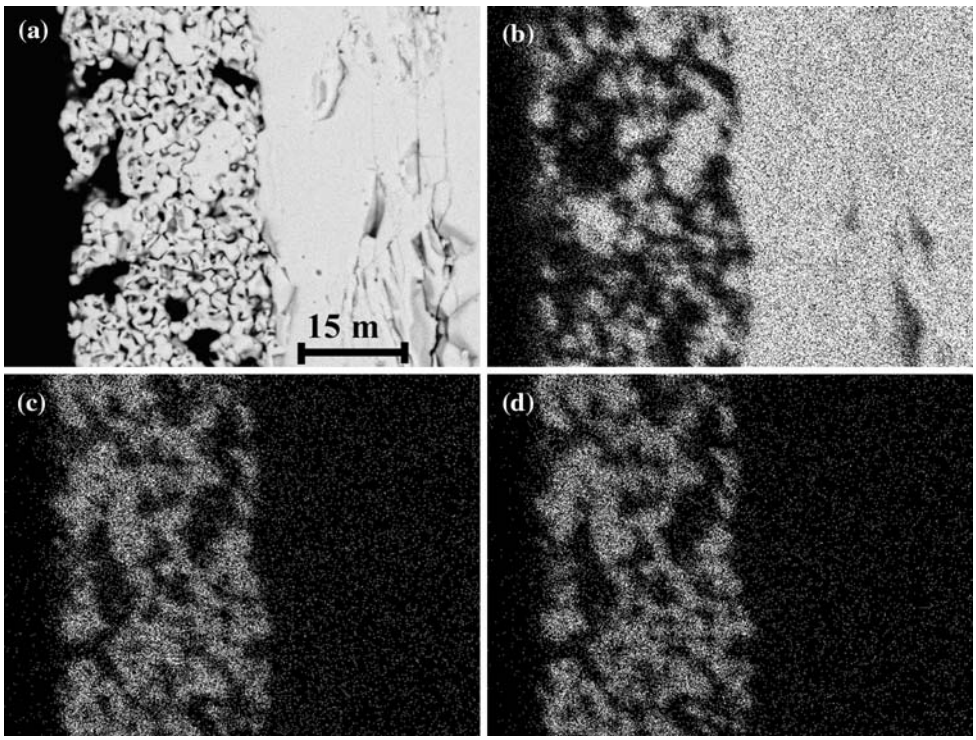

Fig. 4 X-ray maps obtained by EDS on the (Ni–Co)–YSZ cermet after reduction and electrochemical measurements. (**a**) SEM micrograph; (**b**) Zr; (**c**) Co; (**d**) Ni

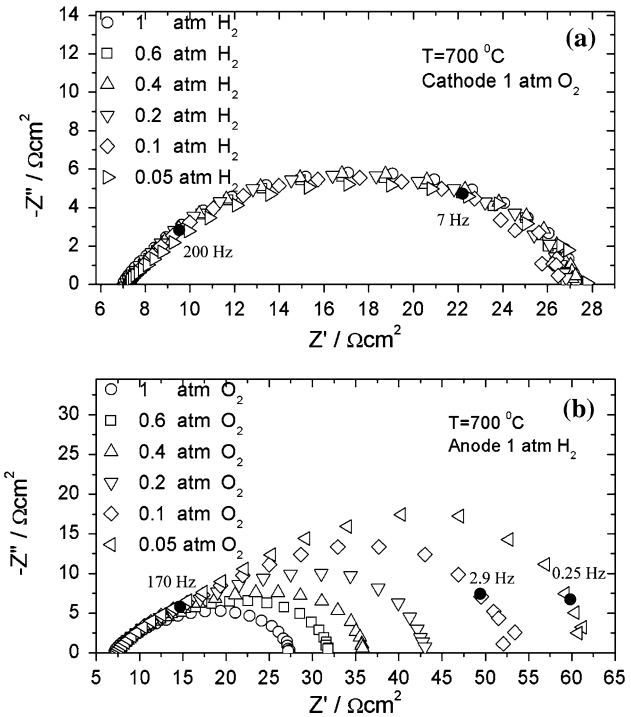

Fig. 5 Nyquist plot obtained with complete cell at 700 °C and under the following conditions: (**a**) 100% O_2 at cathode and varying H_2 partial pressure at anode; (**b**) 100% H_2 at anode and varying O_2 partial pressure at cathode

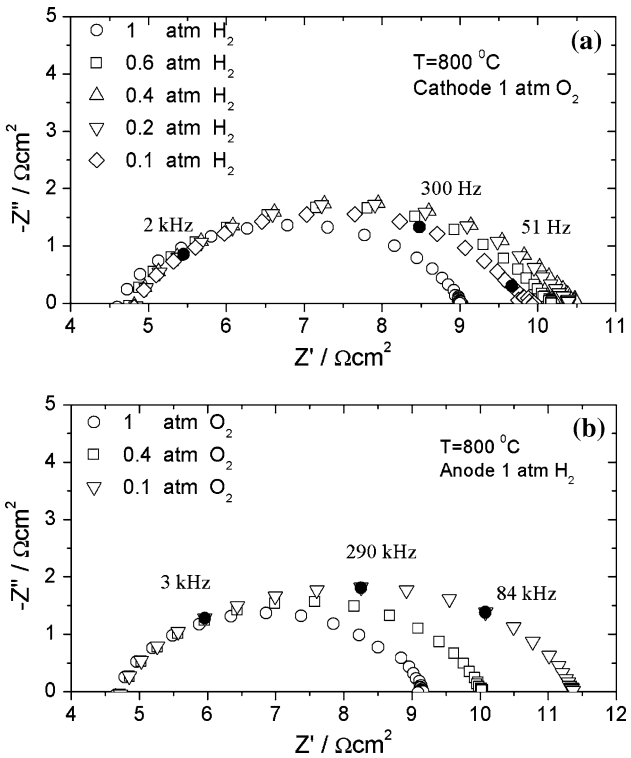

Fig. 6 Nyquist plot obtained with the complete cell at 800 °C and under the following conditions: (**a**) 100% O_2 at cathode and varying H_2 partial pressure at anode; (**b**) 100% H_2 at anode and varying O_2 partial pressure at cathode

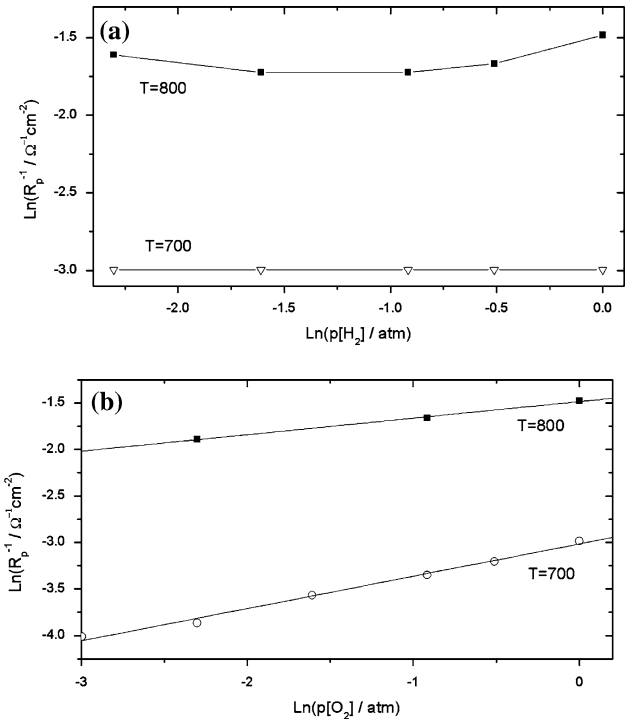

Fig. 7 Dependence on $\ln(p(H_2))$ (**a**) and $\ln(p(O_2))$ (**b**) of $\ln(1/R_p)$ as calculated from spectra reported in Figs. 5 and 6. In (**a**) the dropped lines are guidelines instead in (**b**) they represent the best fit for the experimental data

Figure 7b shows also that at 800 °C the dependence of $\ln(1/R_p)$ on $\ln(p(O_2))$ gives a linear relationship with a slope of 0.18 indicating that, as seen before, the electrochemistry of the overall system at that temperature is controlled by both the cathodic and the anodic reaction.

In Fig. 8 the Arrhenius plot of anodic contribution to R_p^{-1} (the rate of total reaction in the cell) is reported. That quantity was obtained by subtracting from R_p the cathodic contribution, measured in half cell in three electrode configuration and in the same oxygen conditions [27]. From this diagram the apparent activation energy of the anodic process is estimated to be 150 kJ/mol and $1/R_p$ values are in agreement with literature data [10, 12] also reported in the figure.

When methane is supplied at the anode side instead of hydrogen slower cell kinetics is registered. This fact is reflected in the cell behavior when both anodic and cathodic gas compositions are modified (Fig. 9). In fact as shown in Fig. 9a, the anode gas composition starts to affect the cell response already at 700 °C. This remarkable decrease in the anodic rate (proportional to $1/R_p$), when methane is used as fuel, is also found at 800 °C, where a regular change in the Nyquist plots is caused by anodic gas concentration variation (Fig. 10a). At constant methane concentration Nyquist plots do not show any variation for oxygen partial pressure in the range 0.6 ÷ 1 atm, while

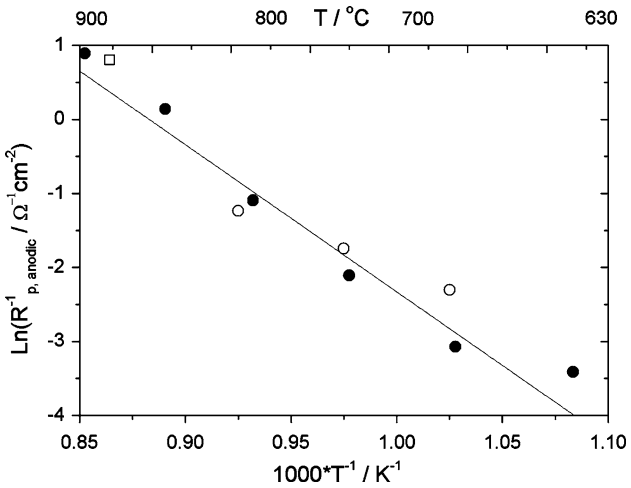

Fig. 8 Temperature dependence of the anodic contribution to R_p^{-1} obtained in pure H_2 and in oxygen partial pressure 0.21 atm (●). The line represents the best fit for the experimental data (Ea = 150 kJ/mol). Moreover the comparison with literature data is presented (□ = [10], ○ = [12])

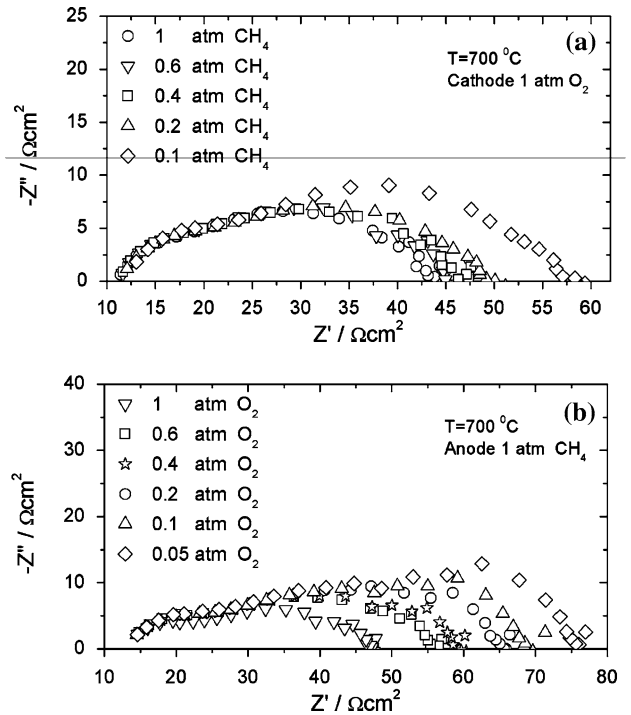

Fig. 9 Nyquist plot obtained with complete cell at 700 °C and under the following conditions: (**a**) with 100% O_2 at cathode and varying at anode partial pressure of CH_4 as reported in figure; (**b**) with 100% CH_4 at anode and varying at cathode partial pressure of O_2 as indicated in figure

increasing resistance is obtained for lower oxygen partial pressure (Fig. 10b). The mixed control of cell kinetics is clearly seen in Fig. 11, where the cell reaction rate is plotted against gas pressures at 700 and 800 °C. In this case

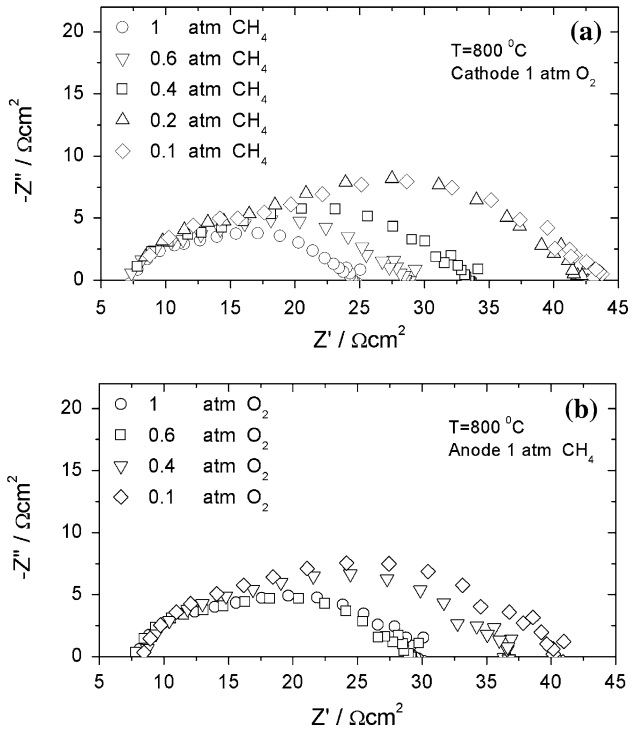

Fig. 10 Nyquist plot obtained with complete cell at 800 °C and for the following conditions: (**a**) with 100% O_2 at cathode and varying at anode partial pressure of CH_4 as reported in figure; (**b**) with 100% CH_4 at anode and varying at cathode partial pressure of O_2 as indicated in figure

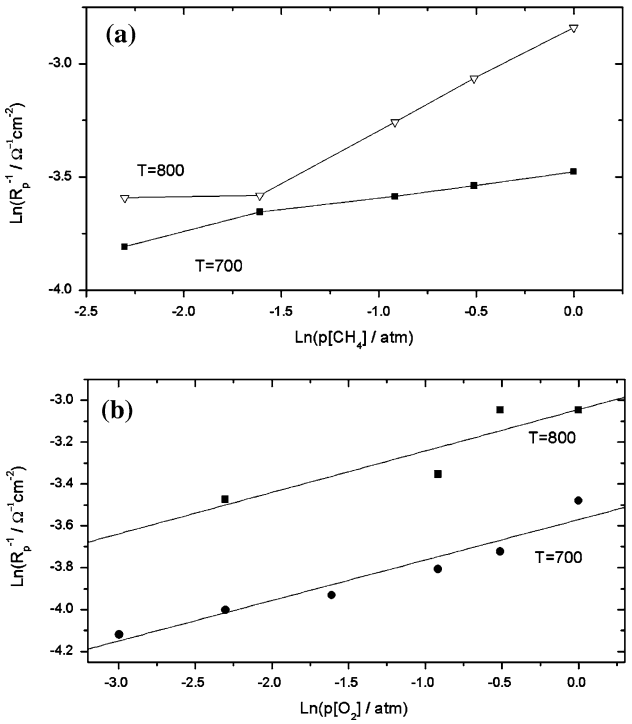

Fig. 11 Dependence on $\ln(p(CH_4))$ and $\ln(p(O_2))$ of $\ln(1/R_p)$ as calculated from OCV impedance spectra obtained with complete cell at 700 and 800 °C and for the following conditions: (**a**) with 100% O_2 at cathode and varying at anode partial pressure of CH_4; (**b**) with 100% CH_4 at anode and varying at cathode partial pressure of O_2. In **a** the dropped lines are guidelines, instead in (**b**) represent the best fit for the experimental data

the dependence of $\ln(1/R_p)$ on $\ln(p(O_2))$ at both temperatures gives a linear relationship with a slope of 0.19. This value is very close to those obtained at 800 °C for hydrogen supplied cell, i.e. under mixed anodic–cathodic control of the overall cell rate. Further considerations about the two electrodic processes can be hardly extracted due to the impossibility to quantitatively separate the anodic and cathodic processes.

Finally, the general behavior of the cells was investigated by *i–V* characteristics measurement. In Fig. 12a, b the results for the hydrogen and methane cells are reported respectively. Maximum power density is observed with hydrogen feeding; at 800 °C about 30 mW/cm^2 were obtained. With methane about 30% less could be obtained at all temperatures in the range 700–900 °C. Power density is lower than values reported in literature for complete cells [12] due to the electrolyte thickness (2 mm). Power lowering under methane could not be ascribed to carbon formation at anode because performance was unchanged during longer testing period (100 h).

However, significant improvements can be expected by optimization of powder synthesis, use of composite cathodes, thin electrolytes and current collecting layers between the platinum net and the cermet anode.

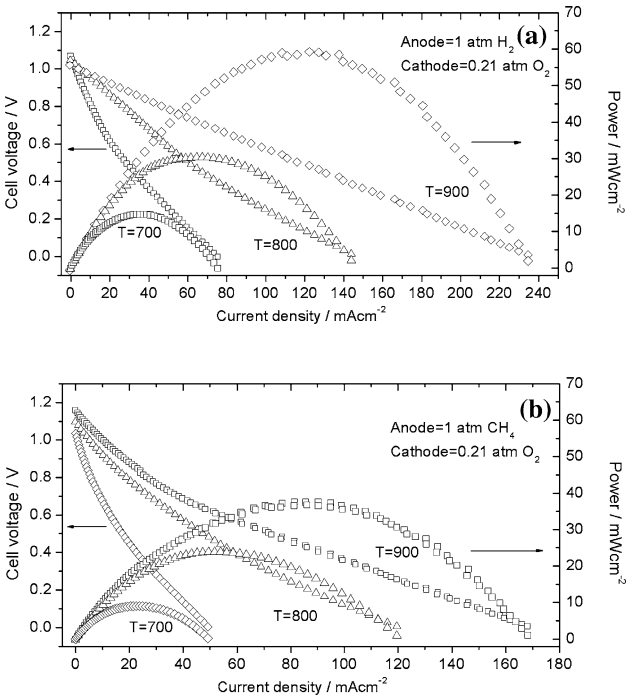

Fig. 12 *I–V* and *i–P* characteristics of complete cell obtained at different temperatures, in oxygen partial pressure 0.21 atm and using as fuel pure H_2 (**a**) or pure CH_4 (**b**)

4 Conclusions

Anodic $Ni_{0.5}Co_{0.5}O$/YSZ powders were prepared by wet impregnation and their characterization was performed by SEM, EDS and XRD. The investigation emphasized a good distribution of $Ni_{0.5}Co_{0.5}O$ and YSZ, and a good porosity after sintering.

The comparison between electrochemical response of the complete SOFC when H_2 or CH_4 is used as fuel was reported. In particular, when CH_4 was used the cell showed higher R_p at all temperatures. A slight worsening was also observed from *i*–*V* curves when CH_4 was the fuel. This behavior can be explained assuming that on switching fuel gas from H_2 to CH_4 and increasing the temperature, the overall system electrochemistry is no longer limited by oxygen reduction but it is under the mixed control of both cathodic and anodic reactions. This work is a further confirmation of the importance of the anode catalytic activity in the design of SOFCs using methane fuel.

Acknowledgement The authors gratefully acknowledge the financial support of the Italian project "FISR 2002: Nanosistemi Inorganici ed Ibridi per lo Sviluppo e l'Innovazione di Celle a Combustibile".

References

1. Minh Q (1993) J Am Ceram Soc 76:563
2. Ormerod RM (2003) Chem Soc Rev 32:17
3. Park S, Vohs JM, Gorte RJ (2000) Nature 404:265
4. Putna ES, Stubenrauch J, Vohs JM et al (1995) Langmuir 11:4832
5. Marina OA, Bagger C, Primdahl S et al (1999) Solid State Ionics 123:199
6. Irvine JTS, Sauvet A (2001) Fuel Cells 1:205
7. He HP, Huang YY, Vohs JM et al (2004) Solid State Ionics 175:171
8. Tao SW, Irvine JTS (2004) Chem Rec 4:83
9. Ringuede A, Labrincha JA, Frade JR (2001) Solid State Ionics 141–142:549
10. Ringuede A, Bronzine D, Frade JR (2002) Electrochim Acta 48:437
11. Ringuede A, Fagg DP, Frade JR (2004) J Eur Ceram Soc 24:1355
12. Sato K, Ohmine Y, Ogasa K, Tsuji S (2003) Solid-solutioning effect of the Ni-based cermet on the electrochemical oxidation of methane. In: Singhal SC, Dokiya M (eds) Proceeding of the international symposium SOFC-VIII. Electrochemical Society, Pennington, pp 695–703
13. Resini C, Herrera Delgado MC, Presto S et al (2008) Int J Hydrogen Energy 33:3728
14. Ringuede A, Bronine D, Frade JR (2002) Solid State Ionics 146:219
15. Keech PG, Trifan DE, Birss V (2005) J Electrochem Soc 152:A645
16. Prabhakaran K, Melkeri A, Beigh MO et al (2007) J Am Ceram Soc 90:622
17. Fukui T, Murata K, Ohara S et al (2004) J Power Sources 125:17
18. Jiang SP, Zhang S, Zhen YD et al (2005) J Am Ceram Soc 88:1779
19. Cracium R, Park S, Gorte RJ et al (1999) J Electrochem Soc 146:4019
20. Park S, Cracium R, Vohs JM et al (1999) J Electrochem Soc 146:3603
21. Bonanos N, Steele BCH, Butler EP (2005) In: Barsoukov E, Macdonald JR (ed) Impedance spectroscopy. Wiley, Hoboken, pp 231–232
22. Moore RJ, White J (1974) J Mater Sci 9:1393
23. Kim JD, Kim GD, Moon JW et al (2001) Solid State Ionics 143:379
24. van Heuveln FH, Bouwmeester HJM (1997) J Electrochem Soc 144:134
25. Barbucci A, Carpanese MP, Viviani M, Vatistas N, Nicolella C (2009) J Appl Electrochem. doi:10.1007/s10800-009-9822-5
26. Nicolella C, Bertei A, Viviani M, Barbucci A (2009) J Appl Electrochem. doi: 10.1007/s10800-008-9691-3
27. Carpanese MP (2003) Degree thesis. University of Genova